Theoretical Investigation of the Hydrogen Abstraction Reaction of the OH Radical with CH_3CHF_2 (HFC152-a): A Dual Level Direct Density Functional Theory Dynamics Study

Mahdi Taghikhani and G. A. Parsafar*

Department of Chemistry, Sharif University of Technology, Tehran 11365-9516, Iran

Hassan Sabzyan

Department of Chemistry, Isfahan University, Isfahan 81746-73441, Iran

Received: May 10, 2005; In Final Form: June 29, 2005

The hydrogen abstraction reaction of the OH radical with CH_3CHF_2 (HFC152-a) has been studied theoretically over a wide temperature range, 200−3000 K. Two different reactive sites of the molecule, CH_3 and CHF_2 groups have been investigated precisely, and results confirm that CHF_2 position of the molecule is a highly reactive site. In this study, three recently developed hybrid density functional theories, namely, MPWB1K, MPW1B95, and MPW1K, are used. The MPWB1K/6-31+G(d,p) method gives the best result for kinetic calculations, including barrier heights, reaction path information and geometry of transition state structures and other stationary points. To refine the barrier height of each channel, a single point energy calculation was performed in MPWB1K/MG3S method. The obtained rate constants by dual level direct dynamics with the interpolated single point energy method (VTST-ISPE) using DFT quantum computational methods, are consistent with available experimental data. The canonical variational transition state theory (CVT) with the zero-curvature and also the small-curvature tunneling correction methods is used to calculate the rate constants. Over the temperature range 200−3000 K, the variation effect, tunneling contribution, branching ratio of each channel are calculated. The rate constants and their temperature dependency in the form of a fitted three-parameter Arrhenius expression are $k_1(T) = 2.00 \times 10^{-19}(T)^{2.24} \exp(-1273/T)$, $k_2(T) = 1.95 \times 10^{-19}(T)^{2.46} \exp(-2374/T)$, and $k(T) = 3.13 \times 10^{-19}(T)^{2.47} \exp(-1694/T)$ cm^3 molecule^{-1} s^{-1}. For the H abstraction from the CHF_2 group, a nonclassical reflection effect is detected as a dominant quantum effect.

Introduction

In recent years, a great number of articles emphasize the role of the haloalkanes in atmosphere.[1−4] The hydrofluorocarbons (HFCs) are a class of chemical substances that have been introduced as ozone friendly alternatives for many industrial usages such as foam blowing, refrigerators and so on, because of the fact that these materials do not take part in the ozone depletion process like chlorofluorocarbons (CFCs) and hydrochloroflourocarbons (HCFCs). In contrast, these compounds have an important role in the greenhouse effect as a result of their high absorption of radiation in the infrared region. Therefore, experimental and theoretical kinetic studies of the HFCs have attracted considerable attention in the past decade. To determine the stability of a HFC species in the troposphere for making appropriate kinetic modeling, its lifetime, rate constant, and temperature dependency, in reaction with various radicals, must be calculated for atmospheric and combustion reactions.

In this study, we have theoretically investigated both mechanism and kinetics of the hydrogen abstraction reaction of OH, as an important radical species in atmospheric and combustion chemistry, with CH_3CHF_2 (HFC-152a). Although the rate constant of the reaction of HFC-152a with OH has been measured by different groups experimentally, its theoretical study has only been done by Uchimaru in 2000.[5] They applied QCISD(T)/6-311G(d,p)//MP2/6-311G(d,p) and PMP2=full/6-311G(3d,2p)//MP2/6-311G(d,p) quantum model build and dynamics modeling of transition state theory with the Eckart and Winger tunneling correction method to evaluate the rate constant, to be consistent with the only available experimental data at 298 K at that time. Their study leads to crude estimation of the rate constant over the temperature range 280−650 K. Girerczak et al.[6] in 1991 and Schemolter et al.[7] in 1993 reported absolute rate constants for the reaction. In 1995, the reaction was also studied by Hsu and DeMore[8] with a relative rate measurement technique. In the recent study, Kozlov et al.[9] measured the total rate constant of reactions over a rather wide temperature range of 210−480 K. In their study, they emphasized the inconsistency of the temperature dependency of the rate constant, which had been reported by the relative and absolute measurement techniques in the previous works. Then, they introduced a new temperature dependency for the rate constant, based on their rather wide range of temperature, by the absolute rate measurement technique. DeMore and coworkers in their recent study have reported the contribution of each reactive site of CH_3CHF_2 in the total rate only at 298 K, experimentally.[10]

Here, we have theoretically studied the reaction between CH_3CHF_2 and OH over a temperature range of 200−3000 K. In the first step, details of the mechanism are reported, in which the reaction path information, thermochemical quantities, barrier heights, and transition state properties for each channel of the reaction are included. Then, in the kinetic calculations, we

* Corresponding author. E-mail: Parsafar@sharif.edu. Tel: +98-21-6165355. Fax: +98-21-6005718.

10.1021/jp0524173 CCC: $30.25
Published on Web 08/20/2005

presented rate constants, tunneling contribution with zero-curvature tunneling (ZCT) and small-curvature tunneling (SCT) correction methods, variation effects, and branching ratios. Various aspects of our investigation are summarized as follows: (1) Three new powerful hybrid density functional methods are applied and compared with ab initio ones to assess their ability in predicting kinetics and thermodynamics properties. (2) Details of the reaction mechanism have been revealed that include the most obscure ones such as transition state geometries, symmetries, and vibrational frequencies as well as degenerate channels of reaction for each site of the molecule. (3) Vigorous statistical theories of reaction dynamics are applied in the calculation of the rate constant and its temperature dependency over a wide temperature range, to include both atmospheric and combustion conditions.

Computational Methods

Electronic Structure Calculations. In this study, we applied one hybrid density functional theory (HDFT) method, namely MPW1K, and two hybrid meta density functional theory methods called MPW1B95 and MPWB1K. In recent publications it has been revealed that the density functional theories (DFT) with adjustable parameters can be applied effectively for kinetic computation. The MPW1K is the modified Perdew−Wang one-parameter model introduced as one of the hybrid density functional theories that can provide a better prediction of energy and geometry than other HDFT methods.[11−13] The two new hybrid meta DFT methods MW1B95 and MPWB1K have been developed in such a way that the functionals depend on the electron density, density gradient, Hartree−Fock exchange, and the Kohn−Sham orbitals in the form of a kinetic energy density, whereas the functionals of the hybrid DFT depend on the electron density, density gradient, and Hartree−Fock exchange only.[14] The MPWB1K method, which was developed for kinetics calculations, has been shown to be more accurate than previously introduced MPW1K method.[14] All mentioned methods have been proposed by Truhlar and coworkers. They have also shown that the results of these kinds of DFT methods are much less sensitive to the basis set than those of ab initio.[15] We have implemented the MPW1K, MPW1B95, and MPWB1K methods with the same 6-31+G(d,p) basis set, besides the MP2/6-311G(d,p) method as an ab initio candidate used for comparison aims. The MPWB1K/6-31+G(d,p) method fulfilled our expectation with the best results for calculated barrier heights, as was asserted by Truhlar group. The minimum energy path (MEP)[16] is constructed with the intrinsic reaction coordinate (IRC) method[17] in mass-weighted Cartesian coordinates with a step size of 0.02 $(amu)^{1/2}$ bohr for each channel of the reaction. We chose the MPWB1K/6-31+G(d,p) method to obtain the geometries, gradients and second derivatives matrix (Hessian matrix) along the minimum energy paths. Furthermore, the MPWB1K level of theory was even reported to have the potential for better prediction for a geometry with a low mean significant error (MSE) than the others.[14] Therefore, the given geometries are accurate enough to be used for the single point energy calculations. For H abstraction from the CHF_2 site, we implement single point energy (SPE) calculations at a high level of theory CCSD(T)/aug-cc-pVTZ to evaluate the barrier height. The CCSD(T) is the couple cluster method, which includes single and double excitations with perturbative treatment of triple excitations.[18] The aug-cc-pVTZ acronym stands for Dunnig's correlation consistent polarized valence triple-ζ basis set with augmentation of diffuse function.[19] Also, the SPE calculation in the fourth-order Möller−Plesset perturbation MP4(SDTQ) level of theory [20] with the same basis set is included for the different channels of reaction. Finally, the barrier heights refined with SPE calculation of the MPWB1K/MG3S method were utilized in dual level direct dynamics calculations. The MG3S basis set is derived from the MG3 basis set by omission of diffuse functions on hydrogens.[15] For the radical species, i.e., the open shell systems, unrestricted wave functions are used in the calculations. Most of the calculation is performed with Gaussian 2003.[21] In the MPW1K case both Gaussian 98[22] and 2003 codes were used to report the magnitude of error in the energy calculation of the modified Perdew−Wang exchange functional.[15,23] The error came from the wrong coding of the Gaussian package and it is important for applied computational chemist to know about its magnitude. The bug exists in all versions of Gaussian 98 through revision A.11.[15] One should note that the recently developed MPWB1K and MPW1B95 methods are not available in Gaussian 98. Even in Gaussian 2003 such methods must be applied with IOP key words.

Rate Constant Calculations. Classical transition state theory rate constant calculation is based on the assumption of quasi-equilibrium between reactants and transition state located on the dividing surface at the saddle point region of the potential energy surface. It means that in this theory the energy profile is the only criterion to determine the location of the transition state (TS) for calculation of the rate constant. Due to this postulate, transition state theory provides only an upper bond for the exact rate constant. From the dynamical point of view, such an overestimation occurs as a result of overcounting trajectories crossing over the dividing surface, which is known as the "re-crossing effect".[24−27] The variational transition state theory (VTST) minimized the error that comes from the re-crossing effect by varying the location of the transition state on the generalized dividing surface.[27] The generalized dividing surface is a hypersurface that intersects MEP perpendicular to it. In the canonical variational transition state (CVT)[24,28−31] version of theory, the partition function can be obtained from the canonical ensemble at a given temperature T. Thus, the thermal rate constant of canonical variational transition state theory $k^{CVT}(T)$ may be formulated as follows:

$$k^{CVT}(T) = \min k^{GT}(T,s) = k^{GT}(T,s^{CVT}(T)) \qquad (1)$$

where s is reaction coordinate parameter that determines location of the generalized dividing surface, $s^{CVT}(T)$ is a specific value of s at which the canonical variational transition state rate constant is calculated, $k^{GT}(T,s)$ is the generalized transition state rate constant that is evaluated at the generalized dividing surface and is expressed as

$$k^{GT}(T,s) = \frac{\delta}{\beta h}\frac{Q^{GT}(T,s)}{\phi^{R}(T)}\exp\{-\beta V_{MEP}(s)\} \qquad (2)$$

Here, $V_{MEP}(s)$ is the classical potential energy along the MEP with its zero of energy on the reactants. Q^{GT} is the canonical partition function of the generalized transition state with its local zero of energy on $V_{MEP}(s)$, Φ^{R} is the reactant's partition function per unit volume, h is Plank's constant, $\beta = (1/k_B T)$ has its usual meaning, and δ is the symmetry factor corresponding to the number of degenerated reaction paths that can also be evaluated as the ratio of the reactant rotational symmetry numbers to that of the transition state. If we neglect coupling of different degree of freedoms, each Q^{GT} and Φ^{R} is approximated byproducts of electronic, vibrational, and rotational partition functions. For Φ^{R}, a relative translational partition function per unit volume

is also included. In the dual level direct dynamics, electronic structure information is obtained from two levels of theory, in which the second higher level method performs in some selected point along the MEP for improvement. Here, dual level direct dynamics[32] with the interpolated single-point energy method[33] (VTST-ISPE) was used. We applied the MPWB1K/6-31+G-(d,p) method as a lower level, and the higher level MPWB1K/MG3S was implemented to refine the heights of barriers.

Quantum Effect. The quantum effect on the motion along the reaction coordinate is included in the dynamics calculations by multiplying the CVT rate constant by a temperature-dependent transmission coefficient as follows:

$$k^{\mathrm{CVT/Y}}(T) = \kappa^{\mathrm{Y}}(T)k^{\mathrm{CVT}}(T) \qquad (3)$$

Y indicates the correction method used for calculation of the transmission coefficient that can be obtained by different tunneling correction methods. The minimum energy path semiclassical adiabatic ground state (MEPSAG) method is appropriate if the principal tunneling path is along the MEP. This approach is also known as the zero-curvature tunneling (ZCT) correction method.[34,35] When tunneling is assumed to occur on the path defined by the classical turning points on the concave side of the MEP, a centrifugal-dominant small curvature semiclassical adiabatic ground state (CD-SCSAG) method can be defined. This method is also known as the small-curvature tunneling (SCT)[36,37] approximation.

In the present study, transition state and canonical variational transition state rate constants with zero-curvature and small-curvature tunneling correction methods have been calculated. All vibrational modes are treated as harmonic oscillators, except for one or two of them, which depend on the channel of the reaction. The lowest vibrational modes are considered as a hindered rotor, and their partition functions are obtained by the hindered rotor approximation.[38,39] For the SCT calculations, the effective reduced mass obtained by a sixth-order Lagrangian interpolation. The Euler single-step integrator[40] with a step size of 0.0003 $(\mathrm{amu})^{1/2}$ bohr is used to follow the MEP. The generalized normal-mode analysis is performed for each 0.003 $(\mathrm{amu})^{1/2}$ bohr. The curvature components of the MEP are calculated by using a quadratic fit (a central finite difference method[27]) to obtain the derivative of the gradient with respect to the reaction coordinate. Two electronic states of the OH radical are included in the calculation of its electronic partition function, with a 140 cm^{-1} splitting ($=637.882 \times 10^{-6}$ hartree) in the $^2\Pi$ ground state. All calculations have been performed with the "POLYRATE version 9.1" package provided by Truhlar and co-workers.[41]

Results and Discussion

A. Electronic Structure Properties. *A-1. Reaction Channels.* Depending on the position that OH attacks, we would expect two distinguishable channels as follows:

Channel 1: hydrogen abstraction from CHF_2

$$CH_3CHF_2 + OH \rightarrow CH_3CF_2 + H_2O \qquad (a)$$

Channel 2: hydrogen abstraction from CH_3

$$CH_3CHF_2 + OH \rightarrow CH_2CHF_2 + H_2O \qquad (b)$$

Transition state structures and radical species involved in the above reactions are illustrated in Figure 1.

One transition state structure (TS) for channel 1 was determined with C_s symmetry. This channel is detected as a dominant channel in all the applied methods of calculation, due to its lowest barrier energy. It is also the most exothermic channel of the reaction. The difference in exothermicity of two diverse channels of reaction is related to the stability of product radical species, CH_2CHF_2 and CH_3CF_2. Despite the high electronegativity of the fluorine atom, it stabilizes a radical to which it is directly connected.[42] Such stability is due to the hyperconjugation effect that comes from coupling a p orbital of fluorine with carbon radical atomic orbitals. Therefore, the high stability of CH_3CF_2 radical leads to the exothermicity of the channel 1. Although the hyperconjugation effect of the hydrogen atom is smaller than that of the fluorine atom, it also has a significant role in stabilizing the CH_2CHF_2 radical. In addition, in the reaction process, the OH radical converts to a more stable H_2O molecule. Hence, we may expect that two channels of the reaction are highly exothermic reactions, which is consistent with our calculation in all utilized methods. For the second channel, we considered two transition state structures with C_1 symmetry, TS-α and TS-β shown in Figure 1, and show they depend on the different environments of the abstracted hydrogen atom in the staggered conformation. The structure in which the hydrogen is located between H and F is represented by TS-α, and the other structure in which H is located between two F atoms is shown as TS-β. The OH group in these structures is orientated toward a F atom. Therefore, in this study, channel 2 itself is divided into two distinguished channels 2-α and 2-β. These two channels are only different in their TS structures. In dynamics calculations, we have shown different behavior of these channels which are due to their barriers and intramolecular hydrogen bonding interactions.

A-2. Comparison of Methods. Reaction properties of channels 1 and 2 such as barrier height, energy change, enthalpy change and free energy change are summarized in Tables 1 and 2. The recently developed MPWB1K method provides an even better estimation of barrier height than the powerful MPW1K method in the kinetic calculation field. For the reactions in CHF_2 and CH_3 sites at 298 K, available experimental data for the activation energy (E_a) are 2.19 and 3.95 kcal/mol, respectively. Our calculated barrier energies with zero-point energy (ZPE) correction in the MPWB1K/6-31+G(d,p) method as a lower level method are obtained to be 1.50, 4.76, and 4.63 kcal/mol for channel 1, channel 2-α, and channel 2-β, respectively. The obtained results are the closest values to the experimental data in our lower level calculations for classical barrier heights (without considering any quantum effect). To improve the barrier heights, we have applied the large MG3S basis set in the MPWB1K method. For comparison, the MP4(SDTQ) level of theory with the too large aug-CC-pVTZ basis set has been implemented. In the channel 1 case, in which an underestimation for the barrier energy is determined, so costly an SPE calculation in the ab initio CCSD(T)/aug-CC-pVTZ method has been implemented to assess the reliability of the MPWB1K results. These ab initio methods with such a large basis set effectively minimized the error from the correlation of electrons and "spin contamination effect", in energy calculations.[43] The obtained barrier energies are reported in Tables 1 and 2 for different channels of the reaction. Astoundingly, as summarized in Tables 1 and 2, the newly proposed MPWB1K/MG3S method provides the best result with lower classical barrier height (except for the MPWB95 method), whereas time-consuming CCSD(T) and MP4(SDTQ) high levels of theory only help us to assess the accuracy of the barrier energy values without any improvement in the barrier height obtained from the MPWB1K method. The barrier energy obtained from the CCSD(T) method is a bit higher

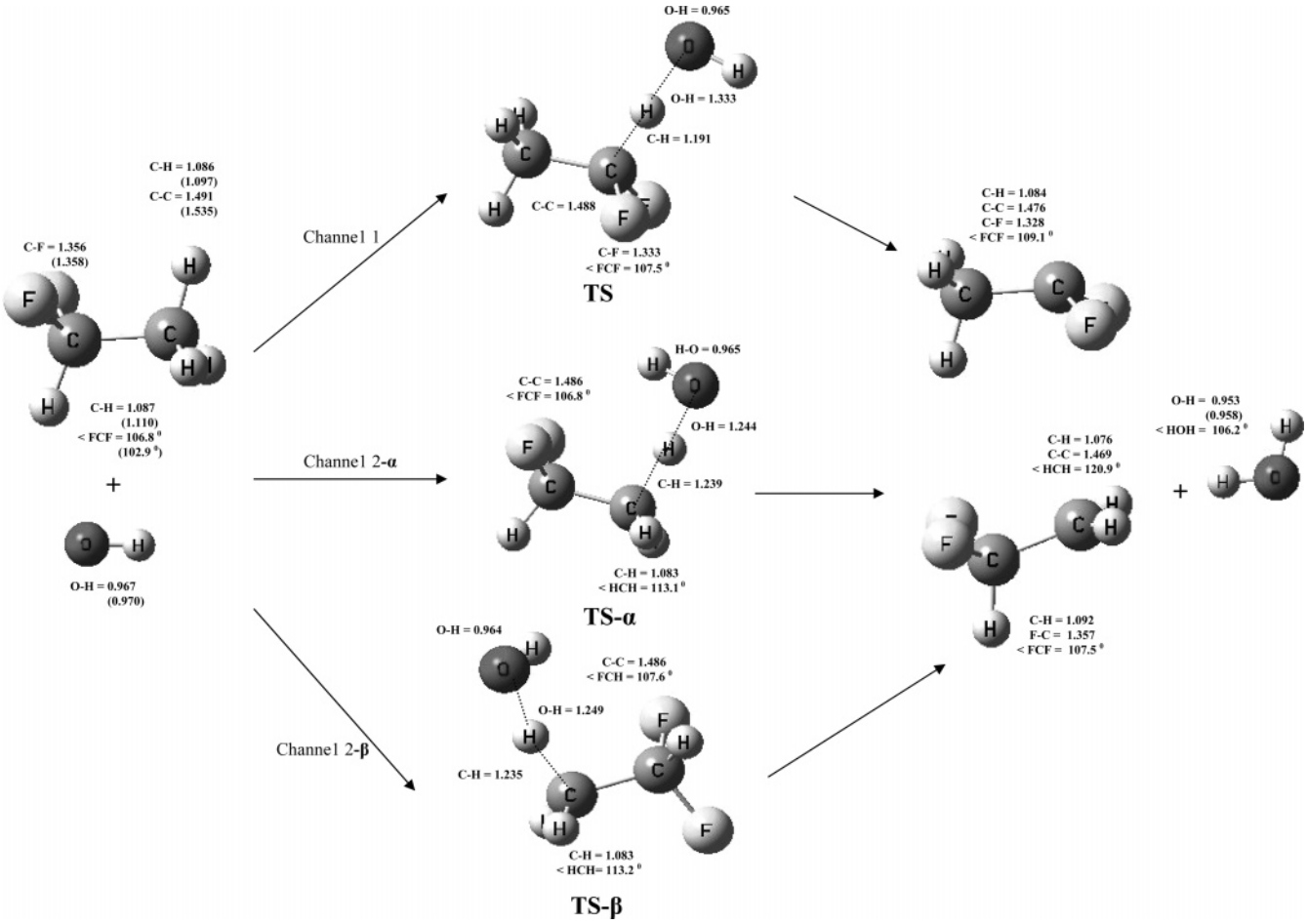

Figure 1. Equilibrium geometry of reactants, products, and transition states at MPWB1K/6-31+G(d,p) level of theory. Bond lengths are in angstroms, and angles are in degrees.

TABLE 1: Properties of Channel 1 [Reaction Energy Changes ΔE_r, Reaction Enthalpy Changes ΔH at 298 K, Classical Barrier Height $V^{\neq}$, Barrier Height of Channel Considering Zero-Point Energy Correction V_A^G, and Reaction Free Energy Changes ΔG_r (All in kcal/mol)]

method	ΔE_r	ΔH (298 K)1	ΔG_r	$V^{\neq}$	V_A^G
MPWB1K/6-31+G(d,p)	−14.96	−14.90	−16.54	3.47	1.50
MPW1K/6-31+G(d,p) -G98[a]	−14.32	−14.24	−15.89	4.28	2.25
MPW1K/6-31+G(d,p) -G03[a]	−14.31	−14.24	−15.89	4.45	2.43
MPWB95/6-31+G(d,p)	−16.88	−16.82	−18.48	0.07	−0.78
MP2/6-311G(d,p)	−16.34			7.76	
MPWB1K/MG3S//MPWB1K/6-31+G(d,p)[b]	−16.70			3.00	1.03
CCSD(T)/aug-cc-pVTZ//MPWB1K/6-31+G(d,p)[b]	−16.03			3.63	1.66
MP4SDTQ/aug-cc-pVTZ//MPWB1K/6-31+G(d,p)[b]	−16.66			5.58	3.61

[a] The MPW1K method implemented with both Gaussian 2003 and Gaussian 98 codes that is labeled as -G98 and -G03 in the table. [b] A//B sign means single point calculation in A's level of theory based on the lower level geometry and frequency calculation of the B's method.

TABLE 2: Properties of Channel 2-α,β [Reaction Energy Changes ΔE_r, Reaction Enthalpy Changes ΔH at 298 K, Classical Barrier Height $V^{\neq}$, Barrier Height of Channel Considering Zero-Point Energy Correction V_A^G, and Reaction Free Energy Changes ΔG_r (All in kcal/mol)]

method	ΔE_r	ΔH (298 K)	ΔG_r	$V^{\neq}$ (ch-α)	$V^{\neq}$ (ch-β)	V_A^G (ch-α)	V_A^G (ch-β)
MPWB1K/6-31+G(d,p)	−9.02	−9.82	−12.02	6.61	6.30	4.76	4.63
MPW1K/6-31+G(d,p) -G98[a]	−9.39	−10.16	−12.66	7.41	7.07	5.38	5.20
MPW1K/6-31+G(d,p) -G03[a]	−9.39	−10.15	−12.67	7.61	7.28	5.58	5.41
MPWB95/6-31+G(d,p)	−10.38	−11.19	−13.48	3.35	3.03	1.55	2.14
MP2/6-311G(d,p)	−10.92			8.99	8.73		
MPWB1K /MG3S//MPWB1K/6-31+G(d,p)[b]	−10.24			6.29	6.09	4.45	4.41
MP4SDTQ/aug-cc-pVTZ//MPWB1K/6-31+G(d,p)[b]	−10.20			6.86	6.55	5.01	4.87

[a] The MPW1K method implemented with both Gaussian 2003 and Gaussian 98 codes that is labeled as -G98 and -G03 in the table. [b] A//B sign means single point calculation in A's level of theory based on the lower level geometry and frequency calculation of the B's method.

than that from MPWB1K/6-31+G(d,p) but very close to it. Because the MPWB1K method is one of the best methods in prediction of TS geometry,[14] especially when long noncovalent interaction exists,[14] the result obtained from the CCSD(T)/aug-CC-pVTZ method affirms the reliability of the calculated barrier energy of MPWB1K. Also the calculated rate constants, at the

TABLE 3: Unscaled Harmonic Vibrational Frequencies (cm^{-1}) and Zero-Point Energies (kcal/mol) for Various Species at MPWB1K/6-31+G(d,p) Level

species	frequencies											ZPE
CH_3CHF_2	3246	3243	3187	3145	1515	1515	1480	1422	1416	1203	1199	39.06
	1184	987	903	576	473	385	237					
	3016[a]	*3001*	*2975*	*2959*	*1457*	*1451*	*1413*	*1364*	*1360*	*1171*	*1145*	
	1135	*942*	*869*	*570*	*471*	*391*	*221*					
CH_3CF_2	3256	3212	3103	1054	1052	1457	1332	1303	1114	1009	898	30.43
	550	469	377	194								
CH_2CHF_2	3394	3266	3125	1487	1412	1405	1209	1194	1020	941	655	29.35
	501	428	395	91								
OH	3868											5.53
	3735											
H2O	4099	3972	1637								13.88	
	3756	*3657*	*1595*									
TS	3895	3258	3239	3141	1511	1503	1471	1426	1315	1263	1219	42.63
	1183	999	932	865	724	527	462	381	224	139	99	
	30	960i										
TS-α	3898	3290	3199	3169	1489	1471	1422	1411	1256	1229	1179	42.75
	1155	980	929	863	713	569	474	416	368	218	125	
	68	1619i										
TS-*β*	3898	3287	3207	3192	1498	1465	1434	1412	1260	1203	1186	42.91
	1168	1027	923	868	706	572	479	406	340	273	123	
	76	1587i										

[a] The italic values are experimental values (for OH and H_2O from ref 50 and for CH_3CHF_2 from ref 51).

MPWB1K/MG3S//MPWB1K/6-31+G(d,p) quantum mechanical model build, are consistent with experimental data.

As summarized in Tables 1 and 2, the MPWB1K and MPW1K methods are better than the commonly used MP_2 method for prediction of barrier height. In the MPW1K method, the wrong coding error of MPW in the Gaussian 98 package causes an underestimation of the barrier heights by as much as 0.1706, 0.2045, and 0.2080 kcal/mol for channel 1, channel 2-α, and channel 2-*β*, respectively. As summarized in Tables 1 and 2, the MPWB95 calculations lead to a meaningless out of range magnitude of barrier heights in comparison to the other applied methods. The values, including the ZPE correction are obtained to be −0.78, +1.55, and +2.14 kcal/mol, for channel 1, channel 2-α, and channel 2-*β*, respectively. In contrast, the MPWB95 method is appropriate for determining thermochemical properties such as energy change, enthalpy change, and free energy change in comparison with the MP_2 and other applied ab initio methods. As shown in Tables 1 and 2, there is a significant difference between the calculated thermodynamic properties obtained from the MPWB95 and the other DFT methods, whereas the obtained results from this method are in agreement with those of ab initio methods for the energy change of the reactions (compare exothermicity of reactions demonstrated in Tables 1 and 2). The obtained results show the accuracy of the MPWB95 method for thermodynamics properties, but not the MPWB1K and MPW1K methods for kinetics (barrier energy) calculations.

Furthermore, spin contamination $\langle S^2 \rangle$ in density functional methods is lower than that of the MP_2 calculations. In the MPWB1K/6-31+G(d,p) method the values of $\langle S^2 \rangle$ are 0.7528, 0.7609, and 0.7525 for OH, TS, and CH_3CF_2; 0.7610 for both TS-α and TS-*β*; and 0.7538 for the CH_2CHF_2 radical. Also, in the last method with the MG3S basis set, the above-mentioned values are somewhat larger and reach values of 0.7529, 0.7609, and 0.7527 for OH, TS, and CH_3CF_2, respectively; 0.7614 for both TS-α and TS-*β*; and 0.7540 for CH_2CHF_2 radical. $\langle S^2 \rangle$ values in the MP_2 calculations are 0.7548, 0.7771, and 0.7561 for OH, TS, and CH_3CF_2, respectively; 0.7808 for both TS-α and TS-*β*; and 0.7807 for CH_2CHF_2 radical.

Finally, and in general, the DFT methods are preferred to ab initio methods because of several advantages. First, the accuracy of the calculated parameters with DFT methods rapidly converge with the size of the basis set. Second, the frequency calculation with the DFT methods does not require too much memory, like ab initio methods. Third, spin contamination errors are small for open shell systems. Fourth, the calculation time is very short. For example, in the energy calculation of the CCSD(T)/aug-CC-pVTZ method for the TS structure of channel 1, CPU timing was ∼47 h on the SGI origin3000 platform using four 400/500 MHz speed cpu's, 32 GB of RAM memory was allocated, and ∼4 GB of dynamic hard disk was used, whereas in the same calculations of the MPWB1K/MG3S method, CPU timing was only about 40 min on the 3200 MHz Intel single processor workstation and less than 500 MB of RAM was used. We only applied the CCSD(T)/aug-CC-pVTZ method for channel 1 of the reaction to confirm the reliability of the MPWB1K barrier energy calculation.

All the aforementioned results should persuade applied chemists to utilize the beneficial and powerful newly developed DFT methods in case studies, especially for large systems.

A-3. Stationary Points. Figure 1 illustrates the equilibrium geometric parameters of the transition states and others stationary points at the lower MPW1K/6-31+G(d,p) level of theory for which frequency calculation and geometry optimization have been performed. The values in parentheses are taken from ref 44. The accurate geometry parameters, as expected, encourage us to use these geometries for higher level SPE calculations. The unscaled frequencies are presented in Table 3 along with available experimental data. First-order TSs are obtained by the Berny[45] algorithm or synchronous transit-guided quasi-newton (STQN)[46,47] method; then they are confirmed with the intrinsic reaction coordinate (IRC) method to be connected with reactants and products. TS-α and TS-*β* refer to channel 2 of the reaction with 0.3013 kcal/mol discrepancy in their energies. Because of low barrier energy values in this case, this minuscule difference should not be neglected, which is 6.52% of the channel 2-α barrier height. In both TS-α and TS-*β*, the OH group is oriented toward a F atom due to the long-range interaction between positive and negative sites. The distances between H and F are 2.444 and 2.546 Å for TS-α and TS-*β*, respectively. The OH orientation plays an important role in determining the reaction path degeneracy for the TSs with C_1 symmetry. Refined classical barrier heights by SPE calculation of the MPWB1K/MG3S

TABLE 4: Calculated CVT/SCT Rate Constants and Branching Ratios along with the Experimental Data for All Channels Involved in the Reaction of OH with HFC-152A

T (K)	k_1	k_2	$k_1 + k_2$	$k_1/(k_1 + k_2)$	$k_2/(k_1 + k_2)$	experimental data[a]
200	8.76E−15	1.03E−15	9.79E−15	0.8948	0.1052	
210	9.67E−15	1.18E−15	1.09E−14	0.8910	0.1090	0.84E−14
220	1.11E−14	1.36E−15	1.25E−14	0.8909	0.1091	0.99E−14
230	1.26E−14	1.57E−15	1.42E−14	0.8894	0.1106	1.19E−14
250	1.61E−14	2.05E−15	1.82E−14	0.8869	0.1131	1.66E−14
272	2.07E−14	2.77E−15	2.35E−14	0.8821	0.1179	2.38E−14
298	2.73E−14	3.88E−15	3.12E−14	0.8755	0.1245	3.38E−14 (5.0E−14)[b]
330	3.72E−14	5.75E−15	4.30E−14	0.8661	0.1339	4.92E−14
370	5.29E−14	9.10E−15	6.20E−14	0.8532	0.1468	7.71E−14
420	7.82E−14	1.53E−14	9.35E−14	0.8365	0.1635	12.05E−14
480	1.19E−13	2.67E−14	1.46E−13	0.8166	0.1834	19.36E−14
500	1.35E−13	3.16E−14	1.67E−13	0.8103	0.1897	
600	2.41E−13	6.79E−14	3.09E−13	0.7802	0.2198	
700	3.94E−13	1.29E−13	5.23E−13	0.7533	0.2467	
800	6.07E−13	2.24E−13	8.31E−13	0.7306	0.2694	
1000	1.26E−12	5.54E−13	1.81E−12	0.6946	0.3054	
1200	2.28E−12	1.14E−12	3.42E−12	0.6663	0.3337	
1500	4.69E−12	2.70E−12	7.39E−12	0.6347	0.3653	
1800	8.39E−12	5.33E−12	1.37E−11	0.6115	0.3885	
2000	1.17E−11	7.82E−12	1.95E−11	0.5994	0.4006	
2500	2.31E−11	1.72E−11	4.03E−11	0.5738	0.4262	
3000	3.95E−11	3.18E−11	7.13E−11	0.5543	0.4457	

[a] Experimental data of Kozlov et al., from ref 9. [b] The given value in parentheses is closest value of theoretical study of Uchimaru et al. in QCISD(T)/6-311G(d,p)//MP2/6-311G(d,p) quantum model build.

method including ZPE corrections are 1.03, 4.45, and 4.41 kcal/mol for channel 1, channel 2-α, and channel 2-β, respectively. Comparison of our results with experimental values of 2.19 and 3.94 kcal/mol for channels 1 and 2 may be confusing in the first step because of the underestimation of the barrier energy in channel 1 before any quantum effects are considered in the rate constant calculation. In other words, the overestimations for channel 2 are reasonable, but the underestimation for channel 1, in which the barrier energy had been estimated with the same MPW1K/6-31+G(d,p) level of theory as a lower level calculation, is baffling in the first step.

For TS, TS-α, and TS-β, the breaking C−H bonds are elongated by 9.57%, 13.97%, and 13.59%, and the forming OH bonds are longer than the equilibrium value of 0.953 Å in H_2O molecule by 39.87%, 30.52%, and 31.01%, respectively. Therefore, three transition state structures are reactant-like, and the saddle points are not located in the middle of the reaction path. In channel 1, the saddle point is located on the reactant side of the reaction path and it is roughly 4 times farther than the product's position, as expected for such an exothermic reaction. The two transition state structures of channel 2 are reactant-like but not as much as that of channel 1. The obtained results validate the relation between exothermicity of the reactions and their saddle point positions on the potential energy surface, known as the "Hammond postulate".[48] TS-β is a bit more reactant-like than TS-α. As shown in Tables 1 and 2, TS-β has a lower energy than TS-α; also both channels correspond to the same reaction energy changes. It means that the TS with the lower barrier is more reactant-like than the other. It divulges the relation between activation energy and location of the transition state structure as proposed by Miller.[49]

B. Dynamics Calculation. *B-1. Rate Constant.* The canonical variational transition state theory with the small-curvature tunneling correction method is utilized to calculate the most accurate thermal rate constant for each channel. The dynamics calculation of the mentioned reactions are carried out with the dual level direct dynamics calculation at the MPWB1K/MG3S//MPWB1K/6-31+G(d,p) density functional theory quantum computational model build. The MEP is taken as a reference path[32] that is constructed with the IRC method at the MPWB1K/6-31+G(d,p) level of theory as a lower level. Up to 30 points in each side of the reaction path (in the reactant and product zones) are used in dynamics calculations for each channel of the reaction. The total rate constant is obtained as the sum of the calculated rate constants ($k^{CVT/SCT}$) of three channels, in which channel 1 corresponds to H abstraction from the CHF_2 position and channel 2-α and channel 2-β both correspond to the H abstraction from the CH_3 position. For each channel, the calculated rate constants based on the transition state theory (TST) and canonical variational transition state theory (CVT) with two tunneling correction methods are compared over a temperature range of 200−3000 K. The variation effects are evaluated as a ratio of the TST rate constant to that of the CVT. Rate constants of channel 1 and 2, their branching ratios and total rate constant in comparison with experimental data at different temperatures are summarized in Table 4.

In channel 1 of the reaction, the two lowest frequency modes (99 and 30 cm^{-1}) of the TS structure, which are located on the saddle point, are considered as hindered rotational modes instead of small amplitude vibrational modes. The modes were removed from the vibrational partition function of the TS and the corresponding hindered rotor partition function, $Q_{HR}(T)$, calculated by the Truhlar method,[37,38] was included in the rate constant expression. The variation effect (k^{TST}/k^{CVT}) for this channel of the reaction varies from 1.887 to 1.759 with temperature. For degeneracy of reaction path, as shown in Figure 1, there is only one way for the OH group to approach the C−H bond of reactant. Therefore, a reaction path degeneracy of 1 is considered for this channel in the calculation of the forward rate constant. Figure 2a depicts the classical potential energy profile ($V_{MEP}(s)$), the vibrationally adiabatic ground state potential energy curve ($V_a^G(s)$), and zero-point energy (ZPE) curve as a function of the intrinsic reaction coordinate s for channel 1.

In channels 2-α and 2-β, direct inspection of the TSs low-frequency modes indicates that only the lowest frequency in each case (68 cm^{-1} for TS-α and 76 cm^{-1} for TS-β) is the hindered internal rotation. For channel 2-α, there are two distinguishable ways for the OH group to approach the C−H bond as a result of OH orientation, whereas for channel 2-β,

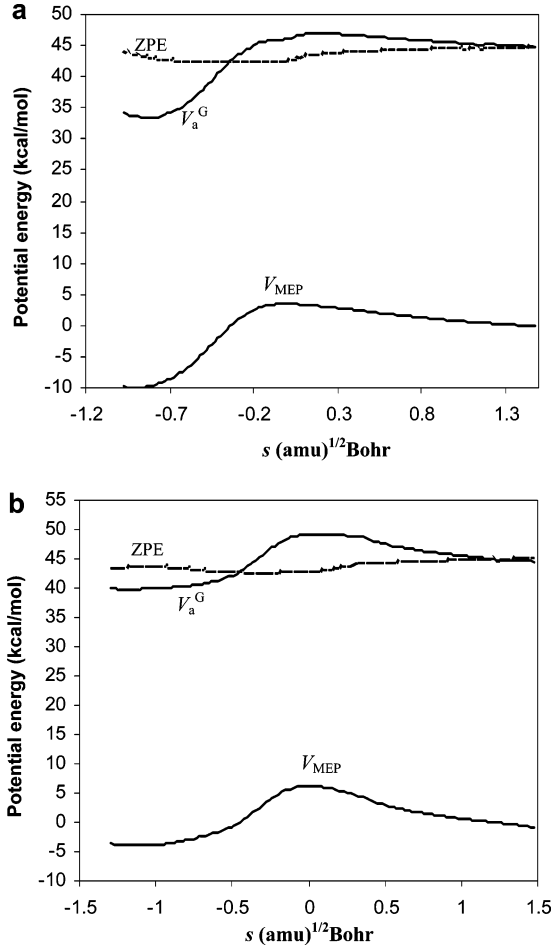

Figure 2. Plots of the classical potential energy ($V_{MEP}(s)$) and the ground state vibrationally adiabatic potential energy ($V_a^G(s)$) of reacting system as function of the intrinsic reaction coordinate s (amu)$^{1/2}$ bohr at the MPWB1K/MG3S//MPWB1K/6-31+G(d,p) level of theory: (a) channel 1; (b) channel 2-β.

for each C−H bond only one way exists for OH to approach and react. Then, due to the fact that there is one reactive C−H bond for TS-α and two for TS-β, the degeneracy of the reaction path for both channels 2-α and 2-β is 2. Figure 2b represents changes of the $V_{MEP}(s)$, $V_a^G(s)$, and ZPE as a function of the intrinsic reaction coordinate s for channel 2-β. The changes of the corresponding quantities for channel 2-α are similar to those in Figure 2b for channel 2-α and, therefore, are not shown. The variation effect (k^{TST}/k^{CVT}) for channel 2-α varies with temperature from 1.328 to 1.2923; for channel 2-β corresponding values are 1.394 and 1.338.

In general, the variation effect for H abstraction reaction seems not to be too important and effective. This fact may be deduced from Figures 2a,b, in which maximum values of $V_{MEP}(s)$ and $V_a^G(s)$ are located approximately at the same position on the reaction path, i.e., at $s = 0$. The zero-point energy, which is the difference of $V_{MEP}(s)$ and $V_a^G(s)$, shows a little change with the reaction coordinate s. This is also more evidence to show that the variation effect is small in this case. The existence of a small variation effect has been frequently reported in a number of articles for H-abstraction reactions.[55−59]

The generalized normal-mode analysis at the nonstationary point along the MEPs, as carried out by diagonalizing the corresponding projected force constant matrix orthogonal to the gradient and six directions, corresponds to translations and rotations.[27] Parts a and b of Figure 3 represent the variation of generalized normal mode vibrational frequencies along the

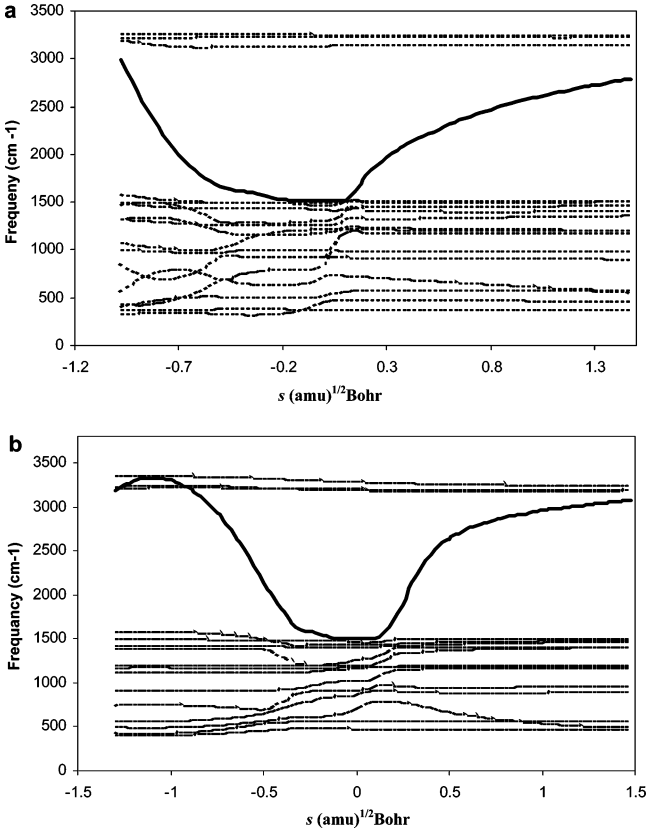

Figure 3. Plots of the generalized normal mode vibrational frequencies (cm^{-1}) as a function of intrinsic reaction coordinate s (amu)$^{1/2}$ bohr: (a) channel 1; (b) channel 2-β.

MEPs of the channel 1 and channel 2-β. Because the corresponding curve for channel 2-α is similar to that of Figure 3b, it is not shown. As shown in Figure 3a, all frequencies, except one, do not change significantly during the reaction process from reactants to products. As shown in this figure, the frequency of one mode changes from 2993 cm^{-1} at $s = +1.5$ (at reactant zone) to 1511 cm^{-1} at $s = 0$ (at the saddle point), and then changes to 2790 cm^{-1} at $s = -1.0$ (at product zone). The nearest values of the reactant and product frequencies are 3187 cm^{-1} (the third mode of CH_3CHF_2) and 3972 cm^{-1} (the second mode of H_2O), which correspond to C−H and O−H stretching, respectively. Direct inspection of animated vibrational mode implies that the mode, which is the fifth mode of the TS structure, transmutes from C−H stretching vibration to the O−H stretching vibration during the reaction process along the MEP. As shown in Figure 3b, a similar behavior exists for the fifth mode of TS-β, in which this mode changes from 3179 to 1498 cm^{-1}, and then to 3069 cm^{-1}. As shown in Figure 3a,b, there is a shift in the location of the U-shape curve of the two mentioned modes, inferring that the TS of channel 1 is more reactant-like than that of the TS-β, as concluded before. Thereby, the appearance of a U-shape curve for one mode can be a typical behavior for all H-abstraction reactions that is due to breaking and forming of a H bond, and crossing over the loose TS structure during reaction process. When we went through published articles to review similar U-shape curves, we found it as a signature for H-abstraction reactions. We must emphasize here that the mentioned mode is a coupled mode with the reaction coordinate not the reactive mode as stated by Luo and Li in dynamics study of CH_2FO.[59]

In Table 4, the CVT/SCT rate constant of channel 1, H abstraction from the CHF_2 group, is shown by k_1. The CVT/SCT rate constant of channel 2, which is the sum of the rate

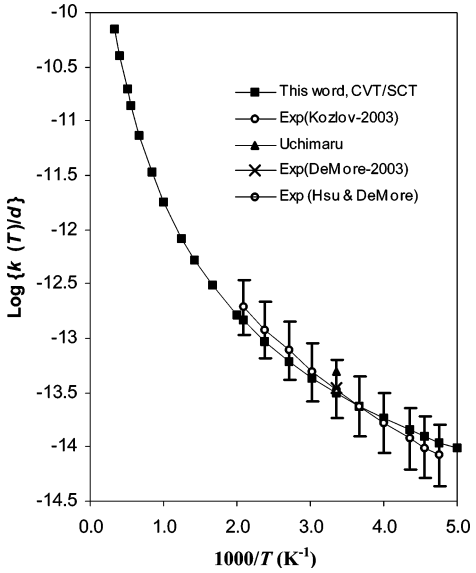

Figure 4. Comparison of the total rate constant obtained from CVT/SCT method with early studies. We considered an error bar of 2% for the data of Kozlov, which is within 1.5−4% amount. In the Introduction, we noted their strategies for measurement. Relative rate constants of DeMore only at 298 K were included, because absolute rate constants for their different reference rate constants were not reported.

constants of channels 2-α and 2-β, is denoted by k_2. The total rate constant is obtained from the sum of k_1 and k_2. The branching ratios of channels 1 and 2 are denoted as $k_1/(k_1 + k_2)$ and $k_2/(k_1 + k_2)$, respectively.

Because of presence of smaller potential barrier, H abstraction from the CHF_2 group is dominant. In the temperature range 200−600 K, the rate constant for attack at the CH_3 group is small and can be neglected. For $T > 600$ K, the rate constant is not negligible. The branching ratios show that even at a high temperature of 3000 K channel 1 is still dominating. Hence, this channel is a major channel of the reaction in the whole temperature range. As discussed in sections A-1 and A-2, channel 1 is the most exothermic channel with the lowest activation energy. Therefore, under both thermodynamically and kinetically controlled conditions, i.e., at high and low temperatures, channel 1 is the more favorable channel. This is consistent with the calculated branching ratios. By the way, the rate constants increase with temperature and the channels become competitive in combustion conditions.

As shown in Figure 4, over the temperature range 210−480 K, the total CVT/SCT rate constant is in agreement with the experimental value. Therefore, our dynamics calculation and quantum computational model built as the VTST-ISPE scheme are accurate enough to produce reliable rate constants.

We should point out here in the study of Uchimaru et al.[5] a kind of error cancellation causing the total rate constant to be in agreement with only available experimental data at 298 K till then. They reported barrier heights on the basis of SPE calculation in QCISD(T)/6-311G(d,p) and PMP2=full/6-311G-(3d,2p), accompanied by frequency calculation in the MP2/6-311G(d,p) method and using a scale factor to obtain thermal energy correction. The reported barrier heights of 3.2, 6.0, and 5.9 kcal/mol, for channels 1, 2-α, and 2-β in the QCISD(T) method and corresponding values of 2.3, 3.6, and 3.4 kcal/mol in the PMP2 method show significant overestimation in comparison with our calculated values of 1.03, 4.45, and 4.41 kcal/mol (section A-3), especially in the channel 1 case. As shown in our study or can be inferred simply from the barrier heights, channel 2 of the reaction is negligible at 298 K, in which

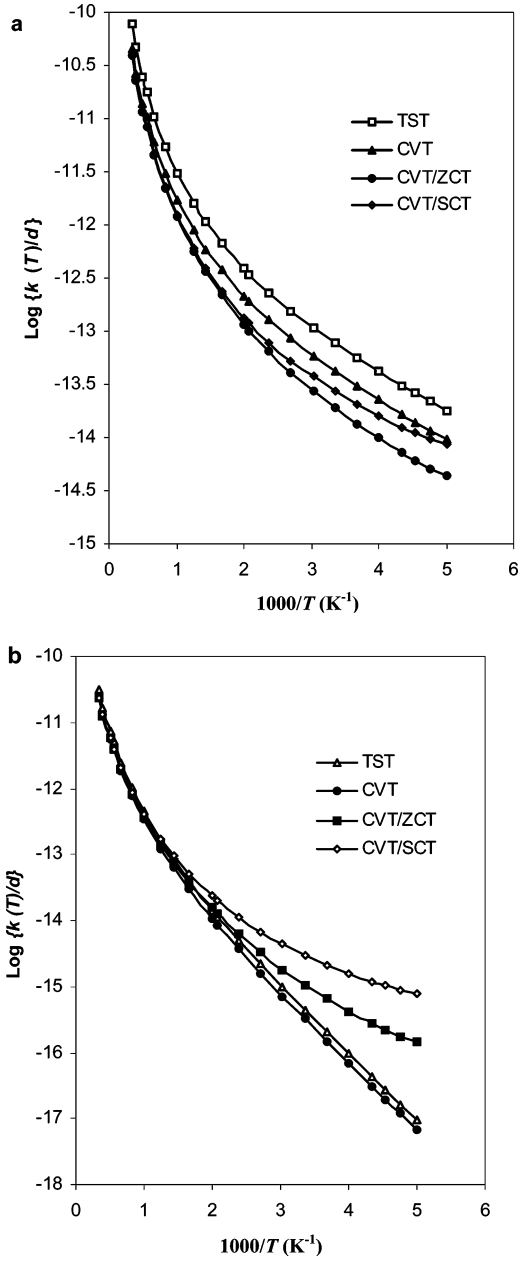

Figure 5. Arrhenius plots of the rate constant calculated (d, cm^3 $molecule^{-1}$ s^{-1}) with the TST, CVT, CVT/ZVT, and CVT/SCT methods versus 1000/T (K^{-1}): (a) channel 1; (b) channel 2-β.

Uchimaru et al. compared their results with experimental data. The error in barrier height calculation causes an underestimation of the rate constant. On the other hand, they overestimated the rate constant on the basis of their unreliable dynamics model built from transition state theory and the Winger tunneling correction method, especially for channel 1 in which an unusual tunneling effect has been identified by the more accurate tunneling correction method in this paper. Hence, in their work, the error cancellation leads to an evaluation of the total rate constant in agreement with experimental data. Moreover, their temperature dependency of the rate constant was not checked as a result of lack of experimental data at that time. That is clear due to exclusion of the hindered rotor mode and their applied tunneling correction method; their temperature dependency of the rate constant that is shown schematically cannot be accurate.

B-2. Tunneling Effect. Panels a and b of Figure 5 demonstrate the importance of quantum effect in the rate constant calculation

of the H abstraction reaction, as expected for such a reaction in which the light H atom transfer is involved. As represented in Figure 5a, for the reaction of channel 1 the quantum effect decreases the rate constant, astonishingly. This is an unusual case of dynamics calculation in which quantum effects preclude particles (supermolecules) to pass over the classical barrier. Detailed analysis of the reactive system shows that this is a special case in which the nonclassical reflection effect, at energies above the barrier, overcomes the tunneling through the classically forbidden region of the barrier. In the classical point of view, the transmission probability for a particle with an energy higher than the barrier height is 1, whereas in the quantum mechanical view the transmission probability is smaller than 1 for the energies above but near the classical barrier energy.[27] In the other words, in the quantum mechanical world, the barrier is not completely transparent for particles. Then, it can reflect back a fraction of particles with an energy higher than the classical barrier or cross through itself a fraction of the particles with energy less than the barrier.

In studied reactions, classical barriers are qualitatively similar in the shape of potential energy surface; however they are not similar quantitatively (Figure 2). For channel 1 of the reaction, the refined barrier energy at the MPWB1K/MG3S level of theory with considering the ZPE correction is only 1.030 kcal/mol. The classical barrier height for channel 1 is about one-fourth of that of channel 2, which is remarkably smaller. It means that with taking into account the thermal distribution, even at a low temperature of 200 K, a high percentage of particles (supermolecules) are unable to tunnel through the classical barrier. In contrast, in this condition the nonclassical reflection effect plays a major role as a quantum effect. And, also, it justifies the underestimation of the classical barrier in comparison with experimental data for channel 1 of the reaction, which is discussed in section A-3.

Figure 5a depicts the TST, CVT, CVT/ZCT, and CVT/SCT rate constants versus 1000/T (K), for channel 1. The difference between TST and CVT curves is due to the variation effect. This effect is less than 2 over the whole temperature range, which is a bit higher than that for the channel 2-β, as depicted in Figure 5b. However, as a result of different scaling of two graphs, this difference is magnified in Figure 5a. The CVT/ZCT curve in which the zero-curvature tunneling correction method is used, represents the lowest rate constant that varies from 4.43E−15 to 3.93E−11 (cm^3 $molecule^{-1}$ s^{-1}) with temperature, whereas the CVT/SCT curve shows almost the same value for the rate constant at high temperature but a higher value at low temperatures. This fact implies that the effect of reaction path curvature becomes important at low temperatures. Hence, at low temperatures, reaction path curvature facilitates the tunneling process to reduce the effect of nonclassical reflection that is in competition with it. At a low temperature of 210 K, the rate constant of channel 2 is negligible, and the CVT/SCT rate constant of channel 1 as a sole channel is in a good agreement with experimental value (see Table 4).

In Figure 5b, the TST, CVT, CVT/ZCT, and CVT/SCT rate constants versus 1000/T (K) are compared with each other, for channel 2-β. In this case, the tunneling effect plays an important role at low temperatures, as expected for such an H abstraction reaction. The barrier for channel 2-β is about 4 times higher than that for channel 1. From here on, tunneling through the barrier in the CVT/SCT theory facilitates the reaction at 200 K, by 110.2305 times with respect to the CVT. As depicted in Figure 5b, from the difference between the CVT/ZCT and CVT/SCT curves, it can be inferred that the reaction path curvature has an essential role in the tunneling process, especially at low temperatures. The TST and CVT curves are near each other for this channel of reaction. For channel 2-α, the same behavior is observed. For this channel at 200 K, the tunneling process increases the rate constant calculated in the CVT/SCT theory, by a factor of 104.7431 in comparison to the CVT theory.

Meanwhile, the TS frequencies of channels 2-α and 2-β are 1619 and 1587 cm^{-1}, respectively (Table 3), from which a crude estimation for width of the barriers may be deduced. The fact that the tunneling for channel 2-α is a bit higher than that for channel 2-β is in accordance with the magnitude of their TS frequencies.

Summary

(1) The accurate rate constant of the reaction was obtained by canonical variational theory with the small curvature tunneling correction method, consistent with experimental data over a wide temperature range, in which a dual level direct density functional theory dynamics as the VTST-ISPE scheme was used. Several evidences confirm that the variation effects are insignificant. On the basis of our calculation, temperature dependencies of the rate constants are

Channel 1: $k_1(T) = 2.00 \times 10^{-19}(T)^{2.24} \exp(-1273/T)$ cm^3 $molecule^{-1}$ s^{-1}

Channel 2: $k_2(T) = 1.95 \times 10^{-19}(T)^{2.46} \exp(-2374/T)$ cm^3 $molecule^{-1}$ s^{-1}

Overall reaction: $k(T) = 3.13 \times 10^{-19}(T)^{2.47} \exp(-1694/T)$ cm^3 $molecule^{-1}$ s^{-1}

(2) The H abstraction from CHF_2 is the dominating channel in the whole 200−3000 K temperature range, including combustion and atmospheric conditions.

(3) Our calculations show that the quantum effects have an important role in evaluation of the rate constant, especially at low temperatures. In channel 1 of the reaction, the quantum effect is reported as the nonclassical reflection effect; such an effect as a dominate quantum effect has not been reported before. Also, contribution of the reaction path curvature to the tunneling effect is evaluated to be essential. The SCT method had been applied by other groups for H-abstraction reaction successfully.[52−61] Although our dynamics calculation with the SCT method has given reliable results for the rate constant, the results motivate more investigations on the quantum effect with a more accurate tunneling correction method such as large curvature tunneling (LCT).[62]

(4) The U-shape curve in the plots of the generalized normal mode vibrational frequencies (Figure 3) is proposed as a characteristic curve for H abstraction reactions. Similar plots are reported in other articles of dynamics studies of H abstraction reactions.[52,55−57,63−65]

Acknowledgment. We thank Professor Donald G. Truhlar for providing the POLYRATE program. The authors also acknowledge University of Waterloo and Professor F. R. McCourt for allowing us to use their hardware and software facilities via telnet. The financial support of the Iranian National Science Foundation and research council of the Sharif University of Technology are appreciated.

Supporting Information Available: Tables S-1−S-3 of forward rate constants of channel 1, channel 2-α, and channel 2-β (all cm^3 $molecule^{-1}$ s^{-1}). This material is available free of charge via the Internet at http://pubs.acs.org.

References and Notes

(1) Tuck, R.; Plumb, A.; Condon, E. *Geophys. Res. Lett.* **1990**, *17*, 313.

(2) Manzer, L. *Science*. **1990**, *249*, 31.
(3) Atkinson, R. *Chem. Rev*. **1986**, *86*, 69.
(4) Good, A. D.; Francisco, S. *J. Chem. Rev.* **2003**, *103*, 4999.
(5) Chandra, A.; Uchimaru, T.; Sugie, M. *J. Comput. Chem* **2000**, *21*, 1305.
(6) Gierczak, T.; Talukdar, R.; Vaghjiani, G. L.; Lovejoy, E. R.; Ravishankara, A. R. *J. Geophys. Res.* **1991**, *96*, 5001.
(7) Schmoltner, A. M.; Talukdar, R. K.; Warren, R. F.; Mellouki, A.; Goldfarb, L.; Gierczak, T.; McKeen, S. A.; Ravishankara, A. R. *J. Phys. Chem.* **1993**, *97*, 8976.
(8) Hsu, K. J.; DeMore, W. B. *J. Phys. Chem*. **1995**, *99*, 11141.
(9) Kozlov, S. N.; Orkin, V. L.; Kurylo, M. J. *J. Phys. Chem. A* **2003**, *107*, 2239.
(10) Wilson, E. W.; Jacoby, A. M, Kukta S. J.; Gilbert, L. E.; Demore W. B. *J. Phys. Chem. A* **2003**, *107*, 9357.
(11) Lynch, B. J.; Fast, P. L.; Harris, M.; Truhlar, D. G. *J. Phys. Chem. A* **2000**, *104*, 4811.
(12) Lynch, B. J.; Truhlar, D. G. *J. Phys. Chem. A* **2001**, *105*, 2936.
(13) Lynch, B. J.; Truhlar, D. G. *J. Phys. Chem. A* **2002**, *106*, 842.
(14) Zhao, Y.; Truhlar, D. G. *J. Phys. Chem. A* **2004**, *108*, 6908.
(15) Lynch, B. J.; Zhao, Y.; Truhlar, D. G. *J. Phys. Chem. A* **2003**, *107*, 1384.
(16) Truhlar, D. G.; Kupperman, A. *J. Am. Chem. Soc.* **1971**, *93*, 1840.
(17) Gonzalez, C.; Schlegel, H. B. *J. Chem. Phys.* **1989**, *90*, 2154.
(18) Raghavachari, K.; Trucks, G. W.; Pople, J. A.; Head-Gordon, M. *Chem. Phys. Lett*. **1989**, *157*, 479.
(19) Woon, D. E.; Dunning, T. H. *J. Chem. Phys.* **1993**, *98*, 1358.
(20) Krishnan, R.; Frisch, M. J.; Pople, J. A. *J. Chem. Phys*. **1980**, *72*, 4244.
(21) Frisch, M. J.; Trucks, G. W.; Schlegel, H. B.; Scuseria, G. E.; Robb, M. A.; Cheeseman, J. R.; Montgomery, J. A., Jr.; Vreven, T.; Kudin, K. N.; Burant, J. C.; Millam, J. M.; Iyengar, S. S.; Tomasi, J.; Barone, V.; Mennucci, B.; Cossi, M.; Scalmani, G.; Rega, N.; Petersson, G. A.; Nakatsuji, H.; Hada, M.; Ehara, M.; Toyota, K.; Fukuda, R.; Hasegawa, J.; Ishida, M.; Nakajima, T.; Honda, Y.; Kitao, O.; Nakai, H.; Klene, M.; Li, X.; Knox, J. E.; Hratchian, H. P.; Cross, J. B.; Bakken, V.; Adamo, C.; Jaramillo, J.; Gomperts, R.; Stratmann, R. E.; Yazyev, O.; Austin, A. J.; Cammi, R.; Pomelli, C.; Ochterski, J. W.; Ayala, P. Y.; Morokuma, K.; Voth, G. A.; Salvador, P.; Dannenberg, J. J.; Zakrzewski, V. G.; Dapprich, S.; Daniels, A. D.; Strain, M. C.; Farkas, O.; Malick, D. K.; Rabuck, A. D.; Raghavachari, K.; Foresman, J. B.; Ortiz, J. V.; Cui, Q.; Baboul, A. G.; Clifford, S.; Cioslowski, J.; Stefanov, B. B.; Liu, G.; Liashenko, A.; Piskorz, P.; Komaromi, I.; Martin, R. L.; Fox, D. J.; Keith, T.; Al-Laham, M. A.; Peng, C. Y.; Nanayakkara, A.; Challacombe, M.; Gill, P. M. W.; Johnson, B.; Chen, W.; Wong, M. W.; Gonzalez, C.; Pople, J. A. *Gaussian 03*, revision B.03; Gaussian, Inc.: Pittsburgh, PA, 2003.
(22) Frisch, M. J.; Trucks, G. W.; Schlegel, H. B.; Scuseria, G. E.; Robb, M. A.; Cheeseman, J. R.; Zakrzewski, V. G.; Montgomery, J. A., Jr.; Stratmann, R. E.; Burant, J. C.; Dapprich, S.; Millam, J. M.; Daniels, A. D.; Kudin, K. N.; Strain, M. C.; Farkas, O.; Tomasi, J.; Barone, V.; Cossi, M.; Cammi, R.; Mennucci, B.; Pomelli, C.; Adamo, C.; Clifford, S.; Ochterski, J.; Petersson, G. A.; Ayala, P. Y.; Cui, Q.; Morokuma, K.; Malick, D. K.; Rabuck, A. D.; Raghavachari, K.; Foresman, J. B.; Cioslowski, J.; Ortiz, J. V.; Stefanov, B. B.; Liu, G.; Liashenko, A.; Piskorz, P.; Komaromi, I.; Gomperts, R.; Martin, R. L.; Fox, D. J.; Keith, T.; Al-Laham, M. A.; Peng, C. Y.; Nanayakkara, A.; Gonzalez, C.; Challacombe, M.; Gill, P. M. W.; Johnson, B. G.; Chen, W.; Wong, M. W.; Andres, J. L.; Head-Gordon, M.; Replogle, E. S.; Pople, J. A. *Gaussian 98*, revision A.7; Gaussian, Inc.: Pittsburgh, PA, 1998.
(23) Adamo, C.; Barone, V. *J. Chem. Phys.* **1998**, *108*, 664.
(24) Truhlar, D. G.; Garrett, B. C. *Annu. Rev. Phys. Chem.* **1984**, *35*, 159.
(25) Truong, T. N. *J. Chem. Phys.* **1994**, *100*, 8014.
(26) Truhlar, D. G.; Fast, P. L. *J. Chem. Phys.* **1998**, *109*, 3721.
(27) Truhlar, D. G.; Isaacson, A. D.; Garrett, B. C. In *Theory of Chemical Reaction Dynamics*; Baer, M., Ed.; CRC Press: Boca Raton, FL, 1985; Vol. 4, Chapter 2.
(28) Truhlar, D. G.; Garrett, B. C. *J. Chem. Phys.* **1987**, *84*, 365.
(29) Baldridge, K. K.; Gordor, M. S.; Steckler, R.; Truhlar, D. G. *J. Phys. Chem.* **1989**, *93*, 5107.
(30) Gonzalez-Lafont, A.; Truong, T. N.; Truhlar, D. G. *J. Chem. Phys.* **1991**, *95*, 8875.
(31) Garrett, B. C.; Truhlar, D. G. *J. Phys. Chem.* **1979**, *83*, 1052.
(32) Truhlar, D. G. Direct Dynamics Method for the Calculation of Reaction Rates. In *The Reaction Path in Chemistry: Current Approaches and Perspectives*; Heidrich, D., Ed.; Kluwer: Dordrecht, The Netherlands, **1995**.
(33) Chuang, Y. Y.; Corchado, J. C.; Truhlar, D. G. *J. Phys. Chem.* **1999**, *103*, 1140.
(34) Truhlar, D. G.; Kuppermann, A. *J. Am. Chem. Soc.* **1971**, *93*, 1840.
(35) Garrett, B. C.; Truhlar, D. G.; Grev, R. S.; Magnuson, A. W. *J. Phys. Chem.* **1983**, *87*, 4554.
(36) Lu, D. h.; Truong, T. N.; Melissas, V. S.; Lynch, G. C.; Liu, Y.-P.; Garrett, B. C.; Steckler, R.; Isaacson, A. D.; Rai, S. N.; Hancock, G.; Lauderdale, J. G.; Joseph, T.; Truhlar, D. G. *Comput. Phys. Comm*. **1992**, *71*, 235.
(37) Liu, Y.-P.; Lynch, G. C.; Truong, T. N.; Dahong, L.; Truhlar, D. G. *J. Am. Chem. Soc*. **1993**, *115*, 2408.
(38) Truhlar, D. G. *J. Comput. Chem.* **1991**, *12*, 266.
(39) Chuang, Y. Y.; Truhlar, D. G. *J. Chem. Phys.* **2000**, *112*, 1221.
(40) Garrett, B. C.; Truhlar, D. G. *J. Phys. Chem.* **1979**, *83*, 3058.
(41) Corchado, Jose C.; Chuang, Yao-Yuan; Fast, Patton L.; Villa, Jordi; Hu, Wei-Ping; Liu, Yi-Ping; Lynch, Gillian C.; Nguyen, Kiet A.; Jackels, Charles F.; Melissas, Vasilios S.; Lynch, Benjamin J.; Rossi, Ivan; Coitino, Elena L.; Ramos, Antonio Fernandez; Pu, Jingzhi; Albu, Titus V.; Department of Chemistry and Supercomputer Institute, University of Minnesota, Minneapolis, Minnesota. POLYRATE version 9.1 (July, 2002).
(42) Jiang, X.; Li, X.; Wang, K. *J. Org. Chem.* **1989**, *57*, 5648.
(43) Szabo, A.; Ostlund, N. S. *Modern Quantum Chemistry;* McGraw-Hill: New York, 1997.
(44) *NIST Standard Reference Database Number 69 − March*, 2003 Release *http://webbook.nist.gov/chemistry/*.
(45) Schlegel, H. B. *J. Comput. Chem*. **1982**, *3*, 214.
(46) Peng, C.; Ayala, P. Y.; Schlegel, H. B.; Frisch, M. J. *J. Comput. Chem.* **1996**, *17*, 49.
(47) Peng, C.; Schlegel, H. B. *Isr. J. Chem.* **1994**, *33*, 449.
(48) Hammond, G. S. *J. Am. Chem. Soc.* **1955**, *77*, 334.
(49) Miller, A. R. *J. Am. Chem. Soc.* **1978**, *100*, 1984.
(50) Chase, M. W., Jr. *NIST-JANAF Themochemical Tables*, 4th ed.; Journal of Physical and Chemical Reference Data; 1998; Monograph 9.
(51) McNaughton, D.; Evans, C. *J. Phys. Chem.* **1996**, *100*, 8660.
(52) Liu, J.; Li, Z.; Dai, Z.; Huang, X.; Sun, C. *J. Phys. Chem. A* **2001**,*105*, 7707.
(53) Masgrau, L.; Gonzalez-Lafont, A.; Lluch, J. M. *J. Phys. Chem. A* **2002**, *106*, 11760.
(54) Espinosa-Garcia, J. *J. Phys. Chem. A* **2002**, *106*, 5686.
(55) Liu, J.; Li, Z.; Dai, Z.; Huang, X.; Sun, C. *J. Phys. Chem. A* **2003**, *107*, 6231.
(56) Sheng, L.; Li, Z.; Liu, J.; Xiao, J.; Sun, C. *J. Phys. Chem. A* **2002**, *106*, 12292.
(57) Zhang, Q.; Wang, S.; Gu, Y. *J. Phys. Chem. A* **2002**, *106*, 3796.
(58) Zhang, Q.; Zhang, R.; Gu, Y. *J. Phys. Chem. A* **2004**, *108*, 1064−1068.
(59) Luo, Q.; Shu Li, Q. *J. Phys. Chem. A* **2004**, *108*, 5050.
(60) Masgrau, L.; Gonzalez-Lafont, A.; Lluch, J. M. *J. Phys. Chem. A* **2003**, *107*, 4490.
(61) Galano, A.; Alvarez-Idaboy, J. R.; Ruiz-Santoyo, Ma. E.; Vivier-Bunge, A. *ChemPhysChem* **2004**, *5*, 1379.
(62) Galano, A.; Alvarez-Idaboy, J. R.; Ruiz-Santoyo, Ma. E.; Vivier-Bunge, A. *J. Phys. Chem. A* **2005**, *109*, 169.
(63) Li, S.; Yu, X.; Xu, Z.; Li, Z.; Sun, C. *J. Phys. Chem. A* **2001**, *105*, 3967. L
(64) Garrett, B. C.; Truhlar, D. J. *J. Am. Chem. Soc.* **1979**, *101*, 4534.
(65) Li, W.; Liu, J.; Li, Z.; Dai, Z.; Huang, X.; Sun, C. *J. Phys. Chem. A* **2003**, *107*, 4921.